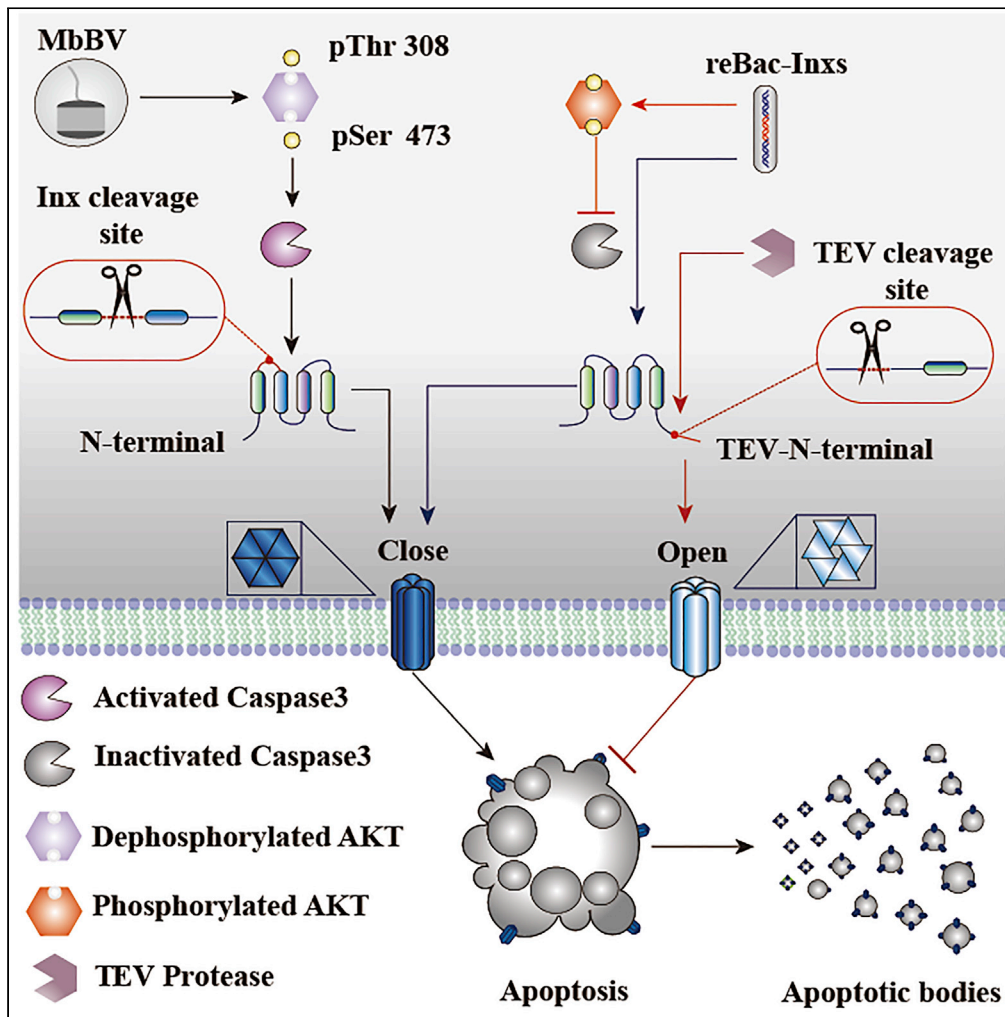## Article

# Bracovirus-mediated innexin hemichannel closure in cell disassembly

Chang-Xu Chen, Hao-Juan He, Qiu-Chen Cai, ..., Wei Xiao, Qi-Shun Zhu, Kai-Jun Luo

kaijun_luo@ynu.edu.cn

### HIGHLIGHTS

Microplitis bicoloratus bracovirus (MbBV) induced apoptotic cell disassembly

Apoptotic body formation accompanied innexin hemichannel closure

MbBV suppressed PI3K/AKT signaling and activated caspase-3

Innexin cleavage by activated caspase-3 was involved in hemichannel closure

# iScience

## Article

# Bracovirus-mediated innexin hemichannel closure in cell disassembly

Chang-Xu Chen,[1,2,3,4] Hao-Juan He,[1,2,3,4] Qiu-Chen Cai,[1,2,3,4] Wei Zhang,[1,2,3,4] Tian-Chao Kou,[1] Xue-Wen Zhang,[1] Shan You,[1] Ya-Bin Chen,[1] Tian Liu,[1,2,3] Wei Xiao,[1,2] Qi-Shun Zhu,[1,2] and Kai-Jun Luo[1,2,3,5,*]

## SUMMARY

**Cell-cell communication is necessary for cellular immune response. Hemichannel closure disrupts communication between intracellular and extracellular environments during polydnavirus-induced immunosuppression in invertebrates. However, the effects of hemichannel closure on cellular immune response are unclear. Here, we examined apoptotic body formation triggered by hemichannel closure in hemocytes of *Spodoptera litura* infected with bracovirus from the parasitic wasp, *Microplitis bicoloratus*. We showed that Microplitis bicoloratus bracovirus (MbBV) induced apoptotic cell disassembly, accompanied by hemichannel closure. Hemocyte apoptotic body formation was caused by the dysregulation of the innexins (Inxs), Inx1, Inx2, Inx3, and Inx4, during the MbBV-mediated inhibition of pI3K/AKT signaling and activation of caspase-3, which cleaved gap junction Inx proteins. Our results showed that hemichannel opening or closure in response to various stimuli, which induces the modulation of Inx levels, could inhibit or activate apoptotic body formation, respectively. Therefore, the "hemichannel open and close" model may regulate the cellular immune response.**

## INTRODUCTION

Immunosuppression occurs during parasitization when endoparasitic wasps inject polydnaviruses into their caterpillar hosts (Bitra et al., 2012; Luo and Pang, 2006; Thoetkiattikul et al., 2005). In some host-parasitoid systems, polydnaviruses induce apoptosis in the host hemocytes (Luo and Pang, 2006; Strand and Pech, 1995). Thus far, the fate of apoptotic hemocytes in this process remains unknown.

It is well known that parasitoid polydnaviruses regulate the host's innate immune response. Humoral and cellular immunity are two arms of the insect innate immune systems, and their functions usually overlap (Stanley and Kim, 2014). Humoral immunity mainly mediates the production of antimicrobial peptides, while cellular immunity destroys pathogens through phagocytosis, nodulation, and encapsulation (Ye et al., 2018). For example, hemocytes kill parasitic eggs by forming a multilayer sheath and encapsulating them (Lavine and Strand, 2002; Stanley et al., 2009); during this process, cell-to-cell communication occurs.

The parasitoid polydnavirus is believed to inhibit cell-to-cell communication to protect the parasitic eggs from the immune response of the lepidopteran host. As early as 1995, it was discovered that the Microplitis demolitor bracovirus (MdBV) induced apoptosis and inactivated hemocytes (Strand and Pech, 1995). Follow-up studies also found the same phenomenon in hemocytes infected by the bracoviruses from *Cotesia congregata*, *Microplitis bicoloratus*, and *Snellenius manilae* (Dong et al., 2017; Le et al., 2003; Tang et al., 2021).

Further studies have shown that polydnaviruses use gene products to induce host hemocyte apoptosis, such as the protein tyrosine phosphatase (PTP) of the bracovirus gene family (Ye et al., 2018). PTP can dephosphorylate target proteins, thereby regulating intracellular signal transmission (Eum et al., 2010; Pruijssers and Strand, 2007; Serbielle et al., 2012). The expression of *PTP-H2* (MdBV) in the Sf21 cell line was found to induce apoptosis (Suderman et al., 2008). Therefore, the regulation of *PTP* in host cell signaling pathways may be one of the ways by which polydnaviruses induce hemocyte apoptosis and inhibit host immune function.

Early studies have described the viral ankyrin gene (*vank*), another member of the bracovirus gene family, as an inhibitor of NF-κB; and similar to IκB, it can inhibit the NF-κB signaling pathway of host cells (Bitra et al.,

[1]School of Life Sciences, Yunnan University, Kunming 650500, P.R. China

[2]Key Laboratory of the University in Yunnan Province for International Cooperation in Intercellular Communications and Regulations, Yunnan University, Kunming 650500, P.R. China

[3]Biocontrol Engineering Research Centre of Crop Disease & Pest in Yunnan Province, Kunming 650500, P. R. China

[4]These authors contributed equally

[5]Lead contact

*Correspondence: kaijun_luo@ynu.edu.cn

https://doi.org/10.1016/j.isci.2021.102281

2012; Gueguen et al., 2013). In our latest study, we showed that the Microplitis demolitor bracovirus (MbBV) vank protein interacts with dorsal interaction protein 3 and inhibits the transcription of the translation initiation factor *eIF4E*, thereby inducing the transcription of downstream target genes, such as *inx2* and *inx3* (Cai et al., 2021). This overexpression of Innexin (Inx) 2 and Inx3 promotes apoptosis in Sf9 and Spli221 cells by activating a low level of caspase-3 (Liu et al., 2013).

Inxs are the structural elements of hemichannels. Decrease in the transcription level of *inx* or increase in the number of Inx proteins affect hemichannel function, depending on the steady state levels of Inx on the cell surface (Pang et al., 2015).

Findings from studies on vertebrates have shown that apoptotic cells form apoptotic bodies, which are rapidly cleared by neighboring phagocytic cells to prevent inflammation (Bellone et al., 1997; Brock et al., 2017). However, the mechanism by which polydnavirus-induced apoptosis mediates cell disassembly is not clearly understood. Recently, we found that hemichannel closure involves an N-terminal, elongated Inx hemichannel (Chen et al., 2016; Guo et al., 2015). Cell-cell communication is inhibited upon hemichannel closure as suppressed immune cells cannot initiate encapsulation, nodulation, or phagocytosis. However, the mechanism underlying apoptosis induction due to blocked cell communication and the fate of apoptotic cells has not been determined. We investigated the formation of apoptotic bodies triggered by hemichannel closure following MbBV infection of hemocytes derived from the host, *Spodoptera litura*, or from cell lines derived from *S. frugiperda* pupal tissue.

## RESULTS

### Hemichannel closure and apoptotic cellular disassembly

To investigate the disassembly of MbBV-induced apoptotic cells forming apoptotic bodies, we used hemocytes of the host, *S. litura*, its cell line, Spli221, and *S. frugiperda*-derived Sf9, which can undergo inducible apoptosis caused by MbBV infection (Figure 1). We unexpectedly observed that MbBV induced the disassembly of Sf9 cells *in vitro* during time-lapse microscopy. Using the same quantity of bracovirus for infection (three wasp equivalents) and increasing the incubation period, we observed that more cells formed apoptotic bodies, some of which could be labeled using Annexin V-FITC and some, like late apoptotic cells, using Annexin V-FITC and propidium iodide (PI) (Figures 1A–1C).

To determine whether this apoptotic induction occurred naturally in the wasp host, *S. litura*, we compared hemocytes from non-parasitized and parasitized hosts 6 days post-parasitization. We found a significantly higher number of apoptotic bodies in the hemocytes from parasitized hosts than in those from non-parasitized hosts (Figures 1D and 1E).

We had previously reported hemichannel closure during reBac-virus infection (Chen et al., 2016; Guo et al., 2015). Hence, to determine whether hemichannel closure occurred during MbBV infection of Sf9 cells, we used TO-PRO-3, which can pass through open hemichannels (Figure 1F), and found that MbBV significantly decreased TO-PRO-3 uptake in a viral-dose-dependent manner (Figures 1H and 1I). Carbenoxolone (CBX) is a pannexin and connexin hemichannel/gap junction inhibitor, which inhibits Sf9 hemichannel opening (Luo and Turnbull, 2011). We determined that both MbBV and CBX inhibited Sf9 hemichannels to similar extents (Figures 1J and 1K).

Based on the information regarding MbBV-induced apoptosis (Luo and Pang, 2006), we tested our hypothesis that hemichannel closure in MbBV-infected cells would persist throughout the apoptotic process triggered by the virus. We performed a set of assays to detect hemichannels in the different stages of apoptosis using PI and Annexin V-labeled FITC in MbBV-infected cells. PI can pass through hemichannels without endocytosis at 4°C for 5 min (Luo and Turnbull, 2011) (Figure 1G). Similar to hemichannel closure by CBX, we observed hemichannel closure during MbBV infection at 12, 24, and 48 hr post-infection (p.i.) (Figures 1L and 1M). Flow cytometric analysis revealed an increase in early apoptotic cells at 12 and 24 hr but not at 48 hr p.i. and a significant increase in late apoptotic cells from 12 to 48 hr p.i. but not 24 hr (Figures 1N and 1O).

Next, we investigated the relationship between hemichannel closure and apoptotic body formation by comparing the effects of CBX, zeocin, an inducer of apoptosis and DNA double-strand breaks (Delacôte et al., 2007), and MbBV. CBX induced membrane blebbing (Figure 1P, Video S1) but did not induce cellular disassembly. Zeocin killed cells but did not induce cellular disassembly (Figure 1P, Video S2). Interestingly,
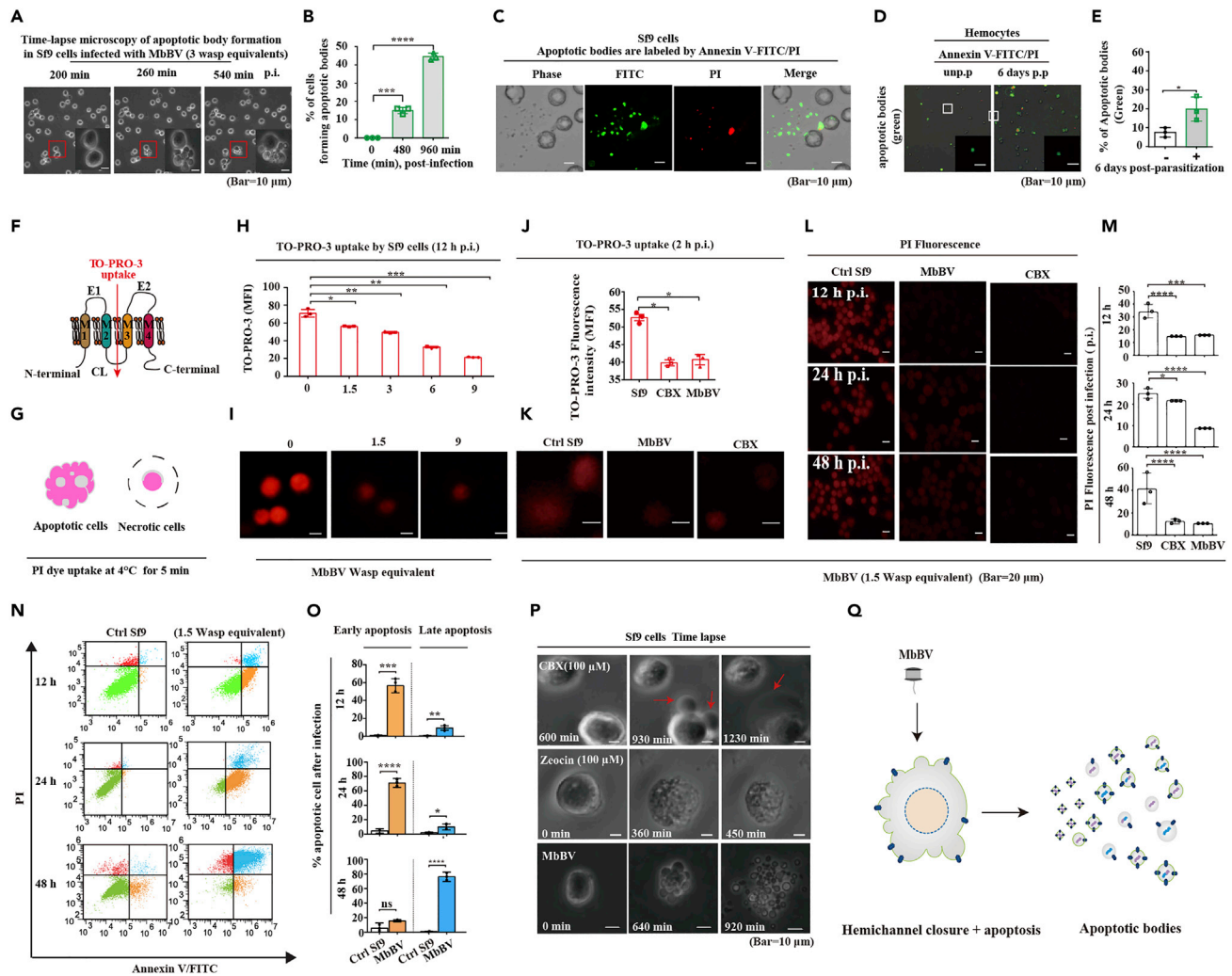
**Figure 1. MbBV triggered apoptotic cell hemichannel closure and disassembly**

(A and B) Time-lapse microscopy of apoptotic body formation triggered by MbBV. The red frame shows cell disassembly. Scale bar, 10 μm; n = 3. ***p < 0.001, ****p < 0.0001, unpaired Student's *t*-test with Holm-Sidak method for multiple *t* test.

(C) Annexin V-FITC/PI labeling of apoptotic bodies. Scale bar, 10 μm.

(D and E) Microscopy of apoptotic body formation triggered by parasitization by the wasp, *Microplitis bicoloratus*, of the host caterpillar, *Spodoptera litura*, using Annexin V-labeled FITC. The white frame shows apoptotic bodies. Scale bar, 10 μm; n = 3.

(F) Schematic of TO-PRO-3 dye uptake from extracellular to intracellular environments through an open hemichannel.

(G) Schematic of the difference between PI uptake by apoptotic and necrotic cells at 4°C for 5 min.

(H and I) MbBV closed the hemichannels in a viral-dosage-dependent manner using TO-PRO-3 uptake. Scale bar, 20 μm; n = 3. *p < 0.05, **p < 0.01, ***p < 0.001, unpaired Student's *t* test with Holm-Sidak method for multiple *t* test.

(J and K) TO-PRO-3 uptake of cells infected by MbBV at 2 hr post-infection (p.i.). Scale bar, 20 μm. Unpaired Student's *t*-test with the Holm-Sidak method for multiple *t* test. Scale bar, 20 μm.

(L and M) PI uptake of cells infected by MbBV at 12, 24, and 48 hr p.i. Scale bar, 20 μm. *p < 0.05, ***p < 0.001, ****p < 0.0001, unpaired Student's *t*-test with Holm-Sidak method for multiple *t* test.

(N and O) Flow cytometric detection of apoptotic Sf9 cells infected by MbBV using Annexin V/PI compared to control (Ctrl). Yellow indicates early apoptosis, and blue indicates late apoptosis. *p < 0.05, **p < 0.01, ***p < 0.001, ****p < 0.0001, unpaired Student's *t*-test with Holm-Sidak method for multiple *t* test; n = 3.

(P) Time-lapse microscopy of cells treated with CBX, zeocin, and MbBV. Scale bar, 10 μm.

(Q) Schematic of apoptotic body formation during hemichannel closure. Cells infected by MbBV showed hemichannel closure and apoptosis and disassembled to form apoptotic bodies.
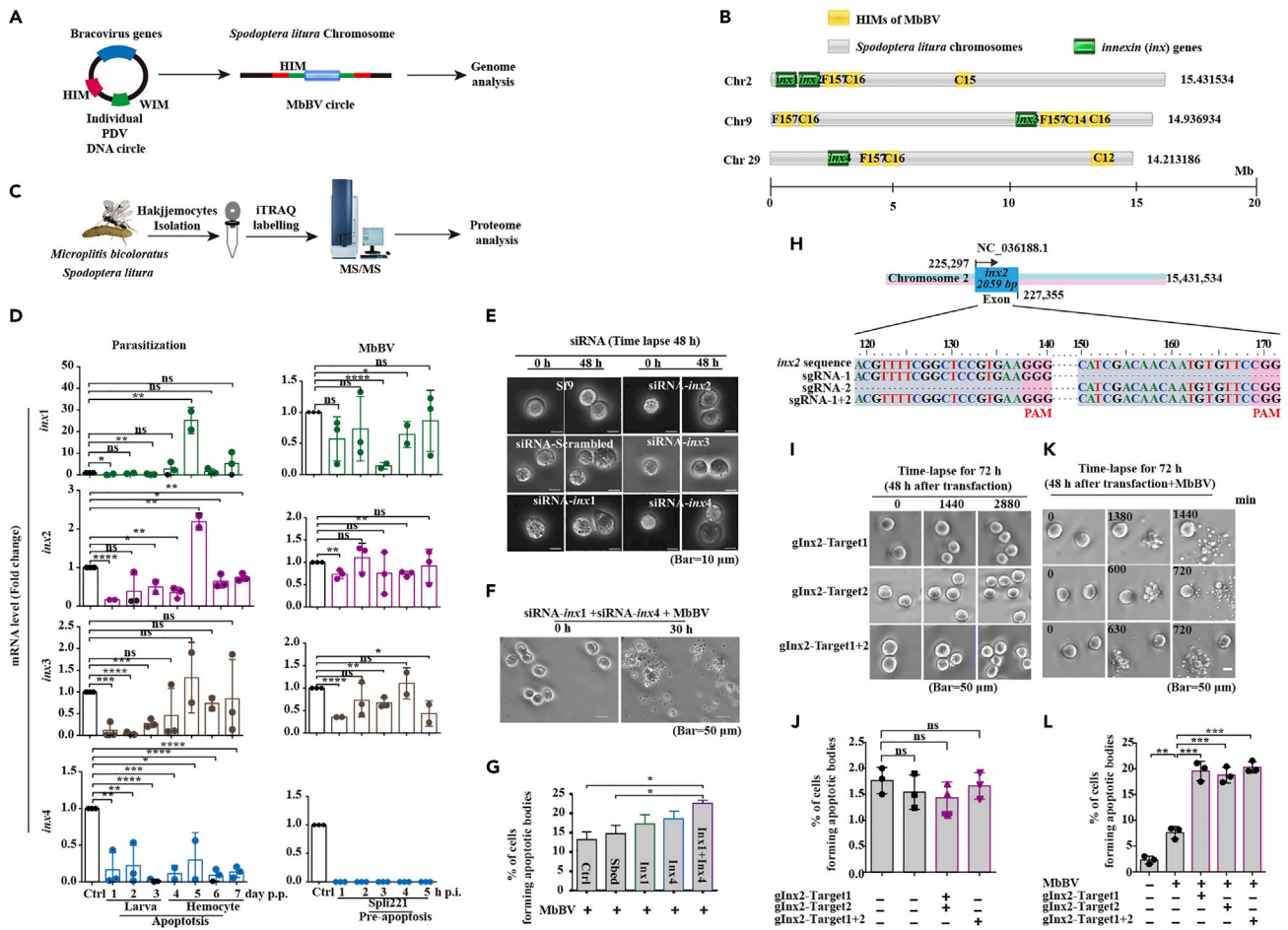
See also Videos S1, S2, and S3.

**Figure 2. MbBV inhibited innexins (Inxs)**

(A) Schematic of MbBV integrated into the genome of *Spodoptera litura* at host integration motifs (HIMs).

(B) Four *inx* genes in chromosomes of *S. litura* and location of viral DNA integration in genome.

(C) Schematic of proteome analysis.

(D) qRT-PCR analysis of the expression of four *inx* genes during natural parasitization (p.p., post-parasitization) and infection by MbBV (p.i., post-infection). Haemocytes in which apoptosis was induced by natural parasitism; Spli221 cells in which pre-apoptosis was induced by infection with MbBV particles. *p < 0.05, **p < 0.01, ***p < 0.001, ****p < 0.0001, ns, no significant differences. Unpaired Student's *t*-test with Holm-Sidak method for multiple *t* test; n = 3.

(E) Time-lapse microscopy of cells treated with siRNA. Scale bar, 10 μm.

(F and G) Time-lapse microscopy of cells treated with siRNA and MbBV.

(H) Schematic of gRNA of *inx2*.

(I–L) CRISPR/Cas9-mediated knockdown of *inx2* in the presence/absence of MbBV infection. Scale bar, 50 μm. The number of cells forming apoptotic bodies. **p < 0.01, ***p < 0.001, ****p < 0.0001, ns, no significant differences. Unpaired Student's *t*-test with Holm-Sidak method for multiple *t* test; n = 3.

See also Figure S1, Tables S1 and S2, and Video S4.

only MbBV induced cell apoptosis and promoted apoptotic cell disassembly (Figure 1P; Video S3). These findings indicate that MbBV induced apoptosis in cells along with the formation of apoptotic bodies, followed by hemichannel closure and the disassembly of cells (Figure 1Q). These results suggest that apoptosis and hemichannel closure are required for apoptotic cell disassembly.

## MbBV inhibited innexins in cell disassembly

Inxs form hemichannels in invertebrates (Güiza et al., 2018; Luo and Turnbull, 2011). To examine the regulation of Inx proteins by MbBV for hemichannel closure, we performed genome analysis (Figure 2A) of *M. bicoloratus*-parasitized hemocytes of *S. litura* and MbBV-infected Spli221 cell line hemocytes by searching for host integration motifs (HIMs) (Beck et al., 2011; Chevignon et al., 2018) to identify the sites of viral integration into host DNA. Four *inx* genes were found in three chromosomes, 2, 9, and 29, among the 31
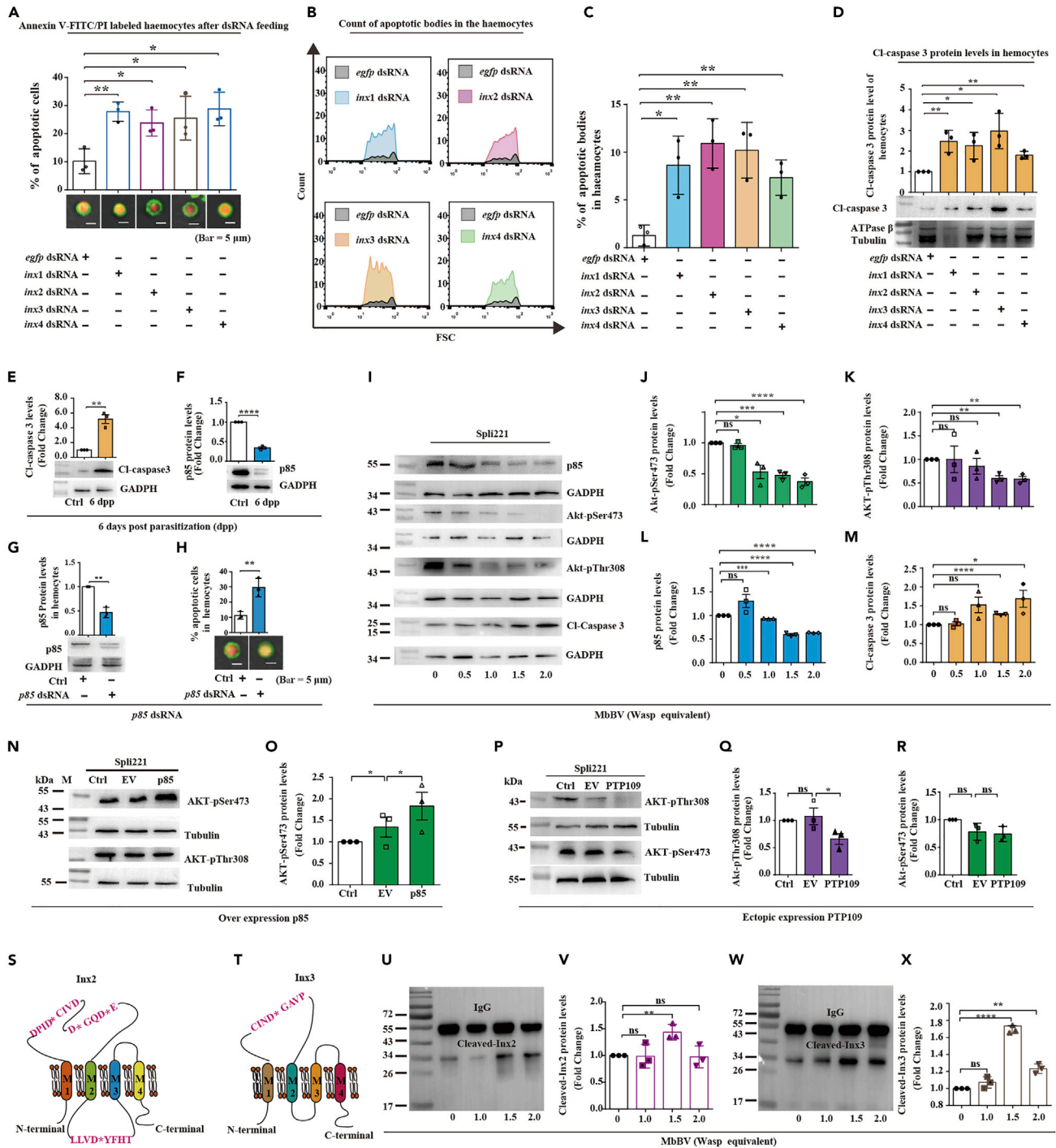
**Figure 3. Innexins (Inxs) are substrates of caspase-3 activated by MbBV**

(A) Annexin V/PI-based detection of apoptotic hemocytes after dsRNA feeding. Scale bar, 5 μm. *p < 0.05, **p < 0.01, unpaired Student's *t*-test with Holm-Sidak method for multiple *t* test; n = 3.

(B and C) Flow cytometric detection of apoptotic bodies in the hemocytes after *inx*-dsRNA feeding. The number of apoptotic bodies after dsRNA feeding to the host. *p < 0.05, **p < 0.01, unpaired Student's *t*-test with Holm-Sidak method for multiple *t* test; n = 3.

(D) Western blot of cleaved (activated) caspase-3 (Cl-caspase-3) after host feeding with 4 *inx*-dsRNA. *p < 0.05, **p < 0.01, unpaired Student's *t* test with Holm-Sidak method for multiple *t* test; n = 3. ATPase beta chain and tubulin as reference.

(E and F) Western blot of Cl-caspase-3 and p85 in hemocytes 6 days post-parasitization (6 dpp). GAPDH was used as reference.

(G and H) dsRNA-mediated knockdown of *p85* and apoptotic cell detection. Scale bar, 5 μm. **p < 0.01, ***p < 0.001, ****p < 0.000; n = 3.

**Figure 3. *Continued***

(I–M) Western blot of p85, AKT-p-Ser473, AKT-p-Thr308, and Cl-caspase-3 levels with different MbBV doses. GAPDH was used as reference. $*p < 0.05$, $**p < 0.01$, $***p < 0.001$, $****p < 0.0001$, ns, no significant differences. Unpaired Student's $t$-test with Holm-Sidak method for multiple $t$ test; n = 3.

(N–R) Western blot of AKT-p-Ser473 and AKT-p-Thr308 after *p85* overexpression. $*p < 0.05$, ns, no significant differences. Unpaired Student's $t$-test with Holm-Sidak method for multiple $t$ test; n = 3.

(S and T) Schematic of caspase-3 cleavage sites.

(U–X) Western blot of cleavage of Inx2 and Inx3 by MbBV and activated caspase-3. $*p < 0.05$, $****p < 0.0001$, ns, no significant differences. Unpaired Student's $t$-test with Holm-Sidak method for multiple $t$ test; n = 3.

See also Figures S2–S4.

pairs of chromosomes in *S. litura* (Cheng et al., 2017). The HIMs, HIM-C16, and HIM-F157 (Figure S1A) were found near *inx1* and *inx2* in chromosome 2, indicating that MbBV DNA was not inserted into *inx1* and *inx2* (Figure 2B). Similarly, HIM-C16, HIM-C14, and HIM-F157 were found near *inx3* in chromosome 9 (Figure 2B), and HIM-C16 and HIM-F157 were found near *inx4* in chromosome 29 (Figure 2B). Therefore, MbBV DNA was not inserted into any of the four *inx* genes, which led us to question whether this location affected *inx* expression (Table S1).

In addition, we performed proteome analysis (Figure 2C) of the hemocytes of *S. litura.* The proteomics data analysis revealed an absence of Inx1 and Inx4 proteins, normal levels of Inx2, and decreased levels of Inx3 (Table S2). To confirm these data, we measured the mRNA levels in hemocytes from *S. litura* larvae after parasitization by the wasp and in Spli221 cells infected by MbBV. *inx1* mRNA could be detected in both the larvae and the hemocytes, albeit inconsistently, and the expression of *inx2* and *inx3* mRNAs was similar, whereas that of *inx4* mRNA was consistently downregulated by MbBV (Figure 2D). The hemocyte expression of *inx1*, *inx2*, and *inx3* was similar in MbBV-infected Spli221 cells; however, no *inx4* mRNA was detected (Figure 2D). Combining the results of the mRNA and protein analyses, we concluded that MbBV downregulated *inx1* and *inx4* expression and inhibited Inx1 and Inx4 synthesis in hemocytes during parasitization and infection by MbBV, whereas *inx2/3* mRNA and protein continued to be expressed.

As these findings led to further questions regarding the roles of Inx1 and Inx4 in apoptotic body formation, we designed siRNAs to knock down the expression of all 4 *inx* genes (Figure S1B). Unexpectedly, none of the siRNAs triggered apoptotic body formation when used alone (Figure 2E, Video S4); however, the treatment of MbBV-infected cells with the combination of siRNAs against *inx1* and *inx4* significantly increased apoptotic body formation (Figures 2F and 2G). To confirm these results, we employed the CRISPR/Cas9 system using *inx2* gRNA (Figure 2H) and found that although no apoptotic bodies were formed when we used gInx2-Target1 and gInx2-Target2, both alone and together (Figures 2I and 2J), apoptotic body formation increased in the presence of both the gRNAs and MbBV infection (Figures 2K and 2L). These results suggest that cooperation between MbBV infection and loss of *inx* is necessary for apoptotic body formation.

## MbBV-pI3K/AKT-caspase-3 modulated Inx expression

To identify the factors responsible for Inx-mediated apoptotic body formation, we generated dsRNAs against all four *inx* genes (Figure S2) by feeding *S. litura* larvae and also determined the levels of apoptosis (Figure 3A) and apoptotic body formation (Figure 3B). We found that all four *inx* dsRNAs increased the number of apoptotic cells (Figure 3A), and flow cytometry analysis (Figure S3) revealed a significant increase in apoptotic body formation (Figures 3B and 3C), which suggests that Inx depletion can trigger apoptosis even in uninfected larvae.

Cleaved caspase-3, which has been found to cleave connexin45.6 (Cx45.6) (Yin et al., 2001), was detected in the hemocytes of larvae after dsRNA administration (Figure 3D). Indeed, cleaved caspase-3 levels were significantly higher (Figure 3E) in hemocytes after parasitization, whereas p85 levels had decreased considerably (Figure 3F). The reduction in p85 levels by treatment with dsRNA directed against the *p85* gene increased the number of apoptotic hemocytes (Figures 3G and 3H). These results led to the investigation of the interaction between the pI3K/AKT signaling pathway, specifically via Ser473 and Thr308 of AKT, and MbBV. We found a viral-dosage-dependent decrease in the levels of AKT-Ser473 phosphorylation (Figures 3I and 3J), AKT-Thr308 phosphorylation (Figure 3K), and p85 (Figure 3L), accompanied by an increased level of cleaved caspase-3 (Figure 3M). To confirm whether p85 phosphorylated AKT-Ser473 and Thr308, we overexpressed *p85* in the Spli221 cell line and found an increase in the levels of AKT-pSer473 but not

of AKT-pThr308 (Figures 3N and 3O), suggesting the involvement of an MbBV-mediated decrease in p85-catalyzed phosphorylation of Ser473 in the observed apoptotic effects.

Next, we investigated the factors from MbBV that could dephosphorylate Thr308. As PTP is known to dephosphorylate Thr308 in AKT and the levels of MbBV PTP109 are high during parasitization, we overexpressed *PTP109* in Spli221 cells and found that AKT-Thr308 was dephosphorylated (Figures 3P and 3Q) to a greater extent than Ser473 (Figure 3R). Taken together, these results indicate that activated (cleaved) caspase-3, generated by MbBV, regulated Inx protein levels, which decreased p85-mediated phosphorylation of AKT-Ser473 and, along with viral PTP109-mediated dephosphorylation of AKT-Thr308, led to the inhibition of the pI3K/AKT signaling pathway.

As Cx45.6 is a substrate of caspase-3 (Yin et al., 2001), we examined whether Inx proteins are also substrates of caspase-3. Interestingly, Inx2 and Inx3 have cleavage sites for caspase-3 (Figures 3S and 3T), and immunoprecipitation results revealed that Inx2 and Inx3 were cleaved by activated caspase-3 (Figures S4A and S4B). Immunoprecipitation results revealed that both activated caspase-3 and MbBV infection led to the cleavage of Inx2 and Inx3 in Spli221 cells (Figures S4C and S4D) to ∼34 kDa fragments. The Spli221 cells showed basal levels of cleaved Inx2 and Inx3 (Figures S4E and S4F) and the cleavage of Inx2 and Inx3 followed a vial-dosage-dependent pattern (Figures 3U–3X). These results indicate that Inx proteins are substrates of activated caspase-3, which is generated by MbBV-mediated cleavage, and that the cleavage of Inx proteins decreased the p85-mediated effects and increased the PTP109-mediated effects on AKT-Ser473 and AKT-Thr308 phosphorylation, respectively.

### Hemichannel opening reduced apoptosis

Based on the above results, we sought to confirm our conclusion that MbBV closed hemichannels by activating caspase-3 to trigger apoptotic cell disassembly. We used reBac-TEV-Inx2 and reBac-TEV-Inx3, which had shown hemichannel closure in infected cells (Chen et al., 2016; Guo et al., 2015), and used a tobacco etch virus (TEV) protease to cleave the TEV sites of the two reBac-TEV-Inxs (Figure 4A). Specifically, cells infected by reBac-TEV-Inxs showed an increase in AKT-pSer473 levels, highly stable AKT-pThr308 levels, and reduced cleavage of caspase-3; resultantly, Inx cleavage was limited (Figures 4B–4G).

Next, in the process of Inx recovery, cell co-infection with reBac-TEV-Inxs and reBac-TEVp resulted in the cleavage of the TEV sites and the loss of a 6×His fragment from the N-terminal ends of the Inx proteins (Figure 4H). All four recovered Inx proteins were detected when the cells were co-infected with both reBac-TEV-Inxs and reBac-TEVp (Figures 4I–4L). Notably, the recovered Inx proteins led to the opening of the Inx hemichannels (Figures 4M and 4N). Simultaneously, the number of apoptotic cells was confirmed to decrease significantly (Figures 4O and 4P), suggesting that the opening of the Inx hemichannels reduced cell disassembly.

Taken together, our results show that MbBV dephosphorylated AKT and activated caspase-3, which cleaved the Inx proteins, closed hemichannels, and promoted apoptotic cell disassembly; additionally, opening of the closed hemichannels reduced the formation of apoptotic bodies (Figure 4Q).

### DISCUSSION

The results of this study enable the advancement of several concepts. First, we identified that MbBV induced hemichannel closure to trigger apoptosis and promote apoptotic cell disassembly. Second, the cleavage of Inxs by activated caspase-3 was responsible for hemichannel closure mediated by MbBV via the suppression of pI3K/AKT signaling. Third, the opening of hemichannels formed by Inxs suppressed apoptosis via the modulation of Inx levels and inhibition of cell-cell communication, which attenuated immunosuppression in invertebrates and vertebrates.

Contrary to the view that the opening of hemichannels mediates apoptosis (Chandrasekhar and Bera, 2012; Hur et al., 2003), our study showed that MbBV promotes the unconventional apoptosis pathway of infected cells. We propose that, in the invertebrate host, the hemichannel switching mechanism is related to cell disintegration, which is consistent with the finding that pannexin1 channel activity is negatively correlated with the number of apoptotic bodies (Poon et al., 2014).
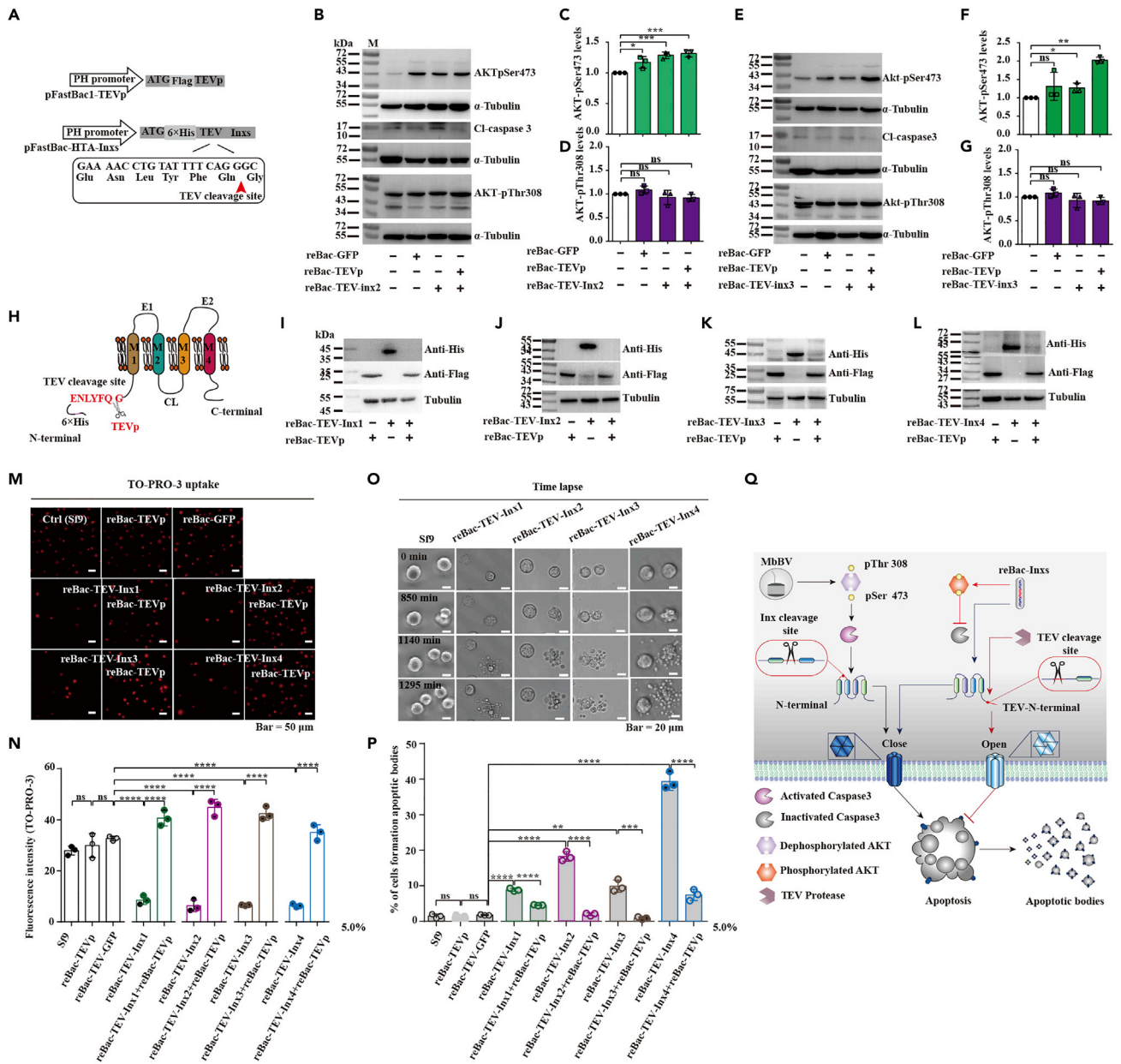
**Figure 4. Reduction in apoptotic body formation upon opening of innexin hemichannel**

(A) Schematic of vectors of reBac-TEV-Inxs and reBac-TEV protease (re-Bac-TEVp).

(B–D) Western blot of AKT-pSer473, AKT-pThr308, and Cl-caspase-3 in cells transduced with reBac-TEV-Inx2 and/or reBac-TEVp. *p < 0.05, **p < 0.01, ***p < 0.001, ****p < 0.0001, ns, no significant differences. Unpaired Student's *t*-test with Holm-Sidak method for multiple *t* test; n = 3.

(E–G) Western blot of AKT-pSer473, AKT-pThr308, and Cl-caspase-3 in cells transduced with reBac-TEV-Inx3 and/or reBac-TEVp cells. *p < 0.05, **p < 0.01, ***p < 0.001, ****p < 0.0001, ns, no significant differences. Unpaired Student's *t*-test with Holm-Sidak method for multiple *t* test; n = 3.

(H) Schematic of TEV cleavage sites in reBac-TEV-Inxs and reBac-TEVp.

(I–L) Western blots of Inxs after co-infection with both reBac-TEV-Inxs and reBac-TEVp.

(M and N) Dye uptake through open hemichannels formed by Inxs after cleavage by TEVp.

(O and P) Time-lapse microscopy of apoptotic bodies after cleavage of Inxs by TEVp; scale bar, 50 μm.

(Q) Schematic of the mechanism of Inx dysregulation by MbBV for the formation of apoptotic bodies via the activation of caspase-3. MbBV promotes pThr308 and pSer473 dephosphorylation to activate caspase-3, which cleaves Inx2 and Inx3, causing apoptotic cell hemichannel closure and forming apoptotic bodies. In contrast, TEV-N-terminal cleavage sites containing reBac-Inxs promote pThr308 and pSer473 phosphorylation to inhibit caspase-3; TEV proteases cleave N-terminal sites to recover Inxs, open hemichannels, and inhibit cell apoptosis.

It is now well known that connexin (Yin et al., 2001) and pannexin (Ruan et al., 2020) are regulated by caspase, and our results also show that Inxs are regulated by caspase-3, completing the mechanism of interaction between the connexin and caspase families. Meanwhile, we also found that MbBV relies on pI3K/AKT signaling to release caspase to induce and accelerate cell apoptosis; this result is different from viruses that also use pI3K/AKT and need to replicate. For example, the enterovirus EV71 activates AKT to inhibit cell apoptosis in the early stages of infection and inhibits AKT phosphorylation to promote cell apoptosis until the late stage of infection (Zhang et al., 2015). This suggests that MbBV may have a different infection mechanism from ordinary viruses and needs to be explored further.

The intercellular transmission of small molecules plays a key role in the regulation of cell tissue homeostasis (Chen et al., 2021). For the immune system, cellular communication mediated by small molecules is particularly important due to the lack of gap junctions. Panx1 has been proven to be widely present in mammalian macrophages (Marina-Garcia et al., 2008), neutrophils (Chen et al., 2010), T cells (Orellana et al., 2013), B cells, and dendritic cells (Saez et al., 2014). Some studies have reported that the main function of the Panx channel is to release ATP (Pelegrin and Surprenant, 2006, 2007). Extracellular ATP is closely involved in the immune response and is usually a pro-inflammatory factor (Faas et al., 2017); however, it may also have anti-inflammatory properties under certain conditions, and its role in the immune response depends on the relative balance between its inflammatory properties (Faas et al., 2017). Therefore, hemichannel closure blocks the transmission of immune signals and inhibits the immune response.

In conclusion, this study revealed a mechanism whereby MbBV-mediated hemichannel closure was activated in MbBV infection-induced immunosuppression during the parasitization of *S. litura* via the inhibition of pI3K/AKT signaling; additionally, apoptosis was also promoted by the activation of caspase-3, a manifestation of the "hemichannel open and close" theory of regulated cellular immune response.

## Limitations of the study

In terms of the limitations, our data are primarily based on the Microplitis bicoloratus bracovirus (MbBV)-*Microplitis bicoloratus-Spodoptera litura* model. Although we confirmed MbBV cellular immunity via hemichannel closure in innate immunity, the regulation of humoral immunity by MbBV may affect hemichannels. Given that the novel "hemichannel opening and closure" model proposes the global regulation between cellular immunity and humoral immunity, further investigation will be necessary to fully understand the molecular mechanisms underlying the link between cellular immunity-hemichannels-humoral immunity in innate immunity during MbBV infection.

## Resource availability

### Lead contact
Further information and requests for resources and reagent should be directed to and will be fulfilled by the lead contact, Kai-Jun Luo (kaijun_luo@ynu.edu.cn).

### Material availability
This study did not generate new unique reagents.

### Data and code availability
This study did not generate data sets.

## METHODS

All methods can be found in the accompanying transparent methods supplemental file.

## SUPPLEMENTAL INFORMATION

Supplemental information can be found online at https://doi.org/10.1016/j.isci.2021.102281.

## ACKNOWLEDGMENTS

## AUTHOR CONTRIBUTIONS

K.L., C.C., H.H., Q.C., T.K., W.Z., W.X., and Q.Z. designed experiments. C.C., W.Z., and X.Z. constructed the L4440 vector and prepared dsRNA feeding. H.H., S.Y., and T.L. constructed CRISPR/Cas9 plasmids. H.H., C.C., and X.Z. constructed bacmids and generated viruses. Q.C. performed genome analysis and proteome analysis. C.C. and Y.C. performed flow cytometry. C.C., H.H., T.K., and S.Y. performed time-lapse experiments. C.C. organized the data. K.L., C.C., Q.C., and X.W. wrote the manuscript. K.L. and W.X. conceived the project.

## DECLARATION OF INTERESTS

The authors declare no competing interests.

## REFERENCES

Beck, M.H., Zhang, S., Bitra, K., Burke, G.R., and Strand, M.R. (2011). The encapsidated genome of Microplitis demolitor bracovirus integrates into the host Pseudoplusia includens. J. Virol. 85, 11685–11696.

Bellone, M., Iezzi, G., Rovere, P., Galati, G., Ronchetti, A., Protti, M.P., Davoust, J., Rugarli, C., and Manfredi, A.A. (1997). Processing of engulfed apoptotic bodies yields T cell epitopes. J. Immunol. 159, 5391–5399.

Bitra, K., Suderman, R.J., and Strand, M.R. (2012). Polydnavirus Ank proteins bind NF-kappaB homodimers and inhibit processing of Relish. PLoS Pathog. 8, e1002722.

Brock, C.K., Wallin, S.T., Mandal, A., Sumner, E.A., and Eisenhoffer, G.T. (2017). Stem cell proliferation is induced by engulfment of apoptotic bodies from adjacent dying cells during epithelial tissue maintenance. Nat. Commun. 28, 1–11.

Cai, Q.-C., Chen, C.-X., Liu, H.-Y., Zhang, W., H, Y.-F., Zhang, Q., Zhou, G.-F., Xu, S., Liu, T., Xiao, W., et al. (2021). Interactions of Vank proteins from Microplitis bicoloratus bracovirus with host Dip3 suppress eIF4E expression. Dev. Comp. Immunol. 118, 103994.

Chandrasekhar, A., and Bera, A.K. (2012). Hemichannels: permeants and their effect on development, physiology and death. Cell Biochem. Funct. 30, 89–100.

Chen, C.-X., Luo, K.-J., Yang, J.-P., Huang, Y.-C., Cardenas, E.R., Nicholson, B.J., and Jiang, J.X. (2021). Connexins and cAMP cross-talk in cancer progression and metastasis. Cancers (Basel) 13, 58.

Chen, Y., Yao, Y., Sumi, Y., Li, A., To, U.K., Elkhal, A., Inoue, Y., Woehrle, T., Zhang, Q., Hauser, C., et al. (2010). Purinergic signaling: a fundamental

mechanism in neutrophil activation. Sci. Signal. 3, ra45.

Chen, Y.-B., Xiao, W., Li, M., Zhang, Y., Yang, Y., Hu, J.-S., and Luo, K.-J. (2016). N-terminally elongated SpliInx2 and SpliInx3 reduce baculovirus-triggered apoptosis via hemichannel closure. Arch. Insect Biochem. Physiol. 92, 24–37.

Cheng, T., Wu, J., Wu, Y., Chilukuri, R.V., Huang, L., Yamamoto, K., Feng, L., Li, W., Chen, Z., Guo, H., et al. (2017). Genomic adaptation to polyphagy and insecticides in a major East Asian noctuid pest. Nat. Ecol. Evol. 1, 1747–1756.

Chevignon, G., Periquet, G., Gyapay, G., Vega-Czarny, N., Musset, K., Drezen, J.-M., and Huguet, E. (2018). Cotesia congregata Bracovirus circles encoding PTP and Ankyrin genes integrate into the DNA of parasitized Manduca sexta hemocytes. J. Virol. 92, e00438-00418.

Delacôte, F., Deriano, L., Lambert, S., Bertrand, P., Saintigny, Y., and Lopez, B.S. (2007). Chronic exposure to sublethal doses of radiation mimetic Zeocin™ selects for clones deficient in homologous recombination. Mutat. Res. 615, 125–133.

Dong, S.-M., Cui, J.-H., Zhang, W., Zhang, X.-W., Kou, T.-C., Cai, Q.-C., Xu, S., You, S., Yu, D.-S., Ding, L., et al. (2017). Inhibition of translation initiation factor eIF4A is required for apoptosis mediated by Microplitis bicoloratus bracovirus. Arch. Insect Biochem. Physiol. 96, e21423.

Eum, J.H., Bottjen, R.C., Pruijssers, A.J., Clark, K.D., and Strand, M.R. (2010). Characterization and kinetic analysis of protein tyrosine phosphatase-H2 from Microplitis demolitor bracovirus. Insect Biochem. Mol. Biol. 40, 690–698.

Faas, M.M., Sáez, T., and de Vos, P. (2017). Extracellular ATP and adenosine: the Yin and

Yang in immune responses? Mol. Aspects. Med. 55, 9–19.

Gueguen, G., Kalamarz, M.E., Ramroop, J., Uribe, J., and Govind, S. (2013). Polydnaviral ankyrin proteins aid parasitic wasp survival by coordinate and selective inhibition of hematopoietic and immune NF-kappa B signaling in insect hosts. PLoS Pathog. 9, e1003580.

Güiza, J., Barría, I., Sáez, J.C., and Vega, J.L. (2018). Innexins: expression, regulation, and functions. Front. Physiol. 9, 1414.

Guo, L.E., Zhang, J.F., Liu, X.Y., Zhang, L.M., Zhang, H.L., Chen, J.H., Xie, X.G., Zhou, Y., Luo, K.-J., and Yoon, J. (2015). Phosphate ion targeted colorimetric and fluorescent probe and its use to monitor endogenous phosphate ion in a hemichannel-closed cell. Anal. Chem. 87, 1196–1201.

Hur, K.C., Shim, J.E., and Johnson, R.G. (2003). A potential role for cx43-hemichannels in staurosporin-induced apoptosis. Cell Commun. Adhes. 10, 271–277.

Lavine, M.D., and Strand, M.R. (2002). Insect hemocytes and their role in immunity. Insect Biochem. Mol. Biol. 32, 1295–1309.

Le, N.T., Asgari, S., Amaya, K., Tan, F.F., and Beckage, N.E. (2003). Persistence and expression of Cotesia congregata polydnavirus in host larvae of the tobacco hornworm, Manduca sexta. J. Insect Physiol. 49, 533–543.

Liu, T., Li, M., Zhang, Y., Pang, Z., Xiao, W., Yang, Y., and Luo, K. (2013). A role for Innexin2 and Innexin3 proteins from Spodoptera litura in apoptosis. PLoS One 8, e70456.

Luo, K., and Turnbull, M.W. (2011). Characterization of nonjunctional hemichannels in caterpillar cells. J. Insect Sci. 11, 6.

Luo, K.-J., and Pang, Y. (2006). Spodoptera litura multicapsid nucleopolyhedrovirus inhibits Microplitis bicoloratus polydnavirus-induced host granulocytes apoptosis. J. Insect Physiol. *52*, 795–806.

Marina-Garcia, N., Franchi, L., Kim, Y.G., Miller, D., McDonald, C., Boons, G.J., and Nunez, G. (2008). Pannexin-1-mediated intracellular delivery of muramyl dipeptide induces caspase-1 activation via cryopyrin/NLRP3 independently of Nod2. J. Immunol. *180*, 4050–4057.

Orellana, J.A., Velasquez, S., Williams, D.W., Saez, J.C., Berman, J.W., and Eugenin, E.A. (2013). Pannexin1 hemichannels are critical for HIV infection of human primary CD4+ T lymphocytes. J. Leukoc. Biol. *94*, 399–407.

Pang, Z., Li, M., Yu, D., Zhang, Y., Liu, X., Ji, X., Yang, Y., Hu, J., and Luo, K. (2015). Two innexins of *Spodoptera litura* influences hemichannel and gap junction functions in cellular immune responses. Arch. Insect Biochem. Physiol. *90*, 43–57.

Pelegrin, P., and Surprenant, A. (2006). Pannexin-1 mediates large pore formation and interleukin-1beta release by the ATP-gated P2X7 receptor. EMBO J. *25*, 5071–5082.

Pelegrin, P., and Surprenant, A. (2007). Pannexin-1 couples to maitotoxin- and nigericin-induced interleukin-1beta release through a dye uptake-independent pathway. J. Biol. Chem. *282*, 2386–2394.

Poon, I.K., Chiu, Y.H., Armstrong, A.J., Kinchen, J.M., Juncadella, I.J., Bayliss, D.A., and

Ravichandran, K.S. (2014). Unexpected link between an antibiotic, pannexin channels and apoptosis. Nature *507*, 329–334.

Pruijssers, A.J., and Strand, M.R. (2007). PTP-H2 and PTP-H3 from Microplitis demolitor Bracovirus localize to focal adhesions and are antiphagocytic in insect immune cells. J. Virol. *81*, 1209–1219.

Ruan, Z., Orozco, I.J., Du, J., and Lu, W. (2020). Structures of human pannexin 1 reveal ion pathways and mechanism of gating. Nature *584*, 646–651.

Saez, P.J., Shoji, K.F., Aguirre, A., and Saez, J.C. (2014). Regulation of hemichannels and gap junction channels by cytokines in antigen-presenting cells. Mediators Inflamm. *2014*, 742734.

Serbielle, C., Dupas, S., Perdereau, E., Hericourt, F., Dupuy, C., Huguet, E., and Drezen, J.M. (2012). Evolutionary mechanisms driving the evolution of a large polydnavirus gene family coding for protein tyrosine phosphatases. BMC Evol. Biol. *12*, 253.

Stanley, D., and Kim, Y. (2014). Eicosanoid signaling in insects: from discovery to plant protection. Crit. Rev. Plant Sci. *33*, 20–63.

Stanley, D., Miller, J., and Tunaz, H. (2009). Eicosanoid actions in insect immunity. J. Innate Immun. *1*, 282–290.

Strand, M.R., and Pech, L.L. (1995). Microplitis demolitor polydnavirus induces apoptosis of a specific haemocyte morphotype in Pseudoplusia includens. J. Gen. Virol. *76*, 283–291.

Suderman, R.J., Pruijssers, A.J., and Strand, M.R. (2008). Protein tyrosine phosphatase-H2 from a polydnavirus induces apoptosis of insect cells. J. Gen. Virol. *89*, 1411–1420.

Tang, C.K., Tsai, C.H., Wu, C.P., Lin, Y.H., Wei, S.C., Lu, Y.H., Li, C.H., and Wu, Y.L. (2021). MicroRNAs from Snellenius manilae bracovirus regulate innate and cellular immune responses of its host *Spodoptera litura*. Commun. Biol. *4*, 52.

Thoetkiattikul, H., Beck, M.H., and Strand, M.R. (2005). Inhibitor kappaB-like proteins from a polydnavirus inhibit NF-kappaB activation and suppress the insect immune response. Proc. Natl. Acad. Sci. U S A *102*, 11426–11431.

Ye, X.Q., Shi, M., Huang, J.H., and Chen, X.X. (2018). Parasitoid polydnaviruses and immune interaction with secondary hosts. Dev. Comp. Immunol. *83*, 124–129.

Yin, X., Gu, S., and Jiang, J.X. (2001). The development-associated cleavage of lens connexin 45.6 by caspase-3-like protease is regulated by casein kinase II-mediated phosphorylation. J. Biol. Chem. *276*, 34567–34572.

Zhang, F., Liu, Y., Chen, X., Dong, L., Zhou, B., Cheng, Q., Han, S., Liu, Z., Peng, B., He, X., et al. (2015). RASSF4 promotes EV71 replication to accelerate the inhibition of the phosphorylation of AKT. Biochem. Biophys. Res. Commun. *458*, 810–815.

# Supplemental information

# Bracovirus-mediated innexin hemichannel

# closure in cell disassembly

Chang-Xu Chen, Hao-Juan He, Qiu-Chen Cai, Wei Zhang, Tian-Chao Kou, Xue-Wen Zhang, Shan You, Ya-Bin Chen, Tian Liu, Wei Xiao, Qi-Shun Zhu, and Kai-Jun Luo

1  **iScience**
2

3  **Supplemental Information**

4
5
6
7

8  **Bracovirus-mediated innexin-hemichannel closure in cell disassembly**

9
10
11  Chang-Xue Chen, Hao-Juan He, Qiu-Chen Cai, Wei Zhang, Tian-Chao Kou, Xue-Wen
12  Zhang, Shan You, Ya-Bin Chen, Tian Liu, Wei Xiao, Qi-Shun Zhu, Kai-Jun Luo
13
14
15
16
17
18
19
20
21
22
23
24
25
26
27
28
29
30
31
32
33
34
35
36
37
38
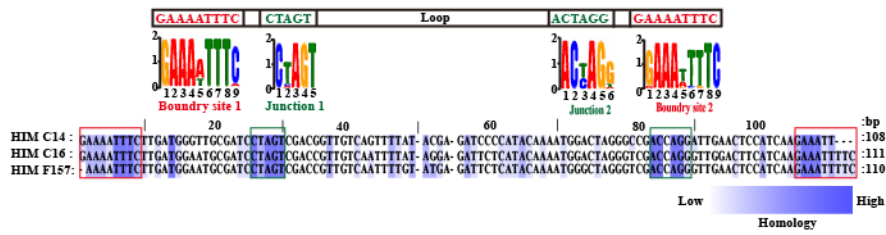39
40
41
42

43

**Figure S1. Host integration motifs (HIMs) and siRNA (Related to Figure 2)**

45 (A) HIM in C14, C16, and F157. (B) Levels of the four Inx proteins after siRNA-dose-

46 dependent knockdown.

47
48
49
50
51
52
53
54
55
56
57
58
59
60
61
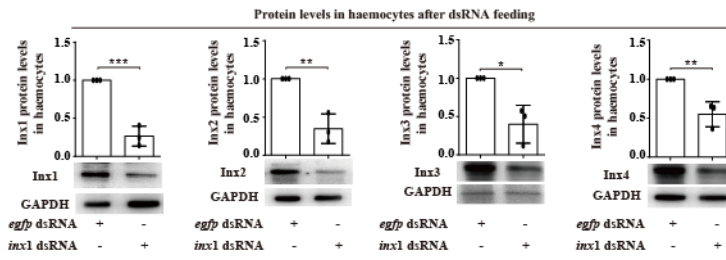62
63
64
65
66
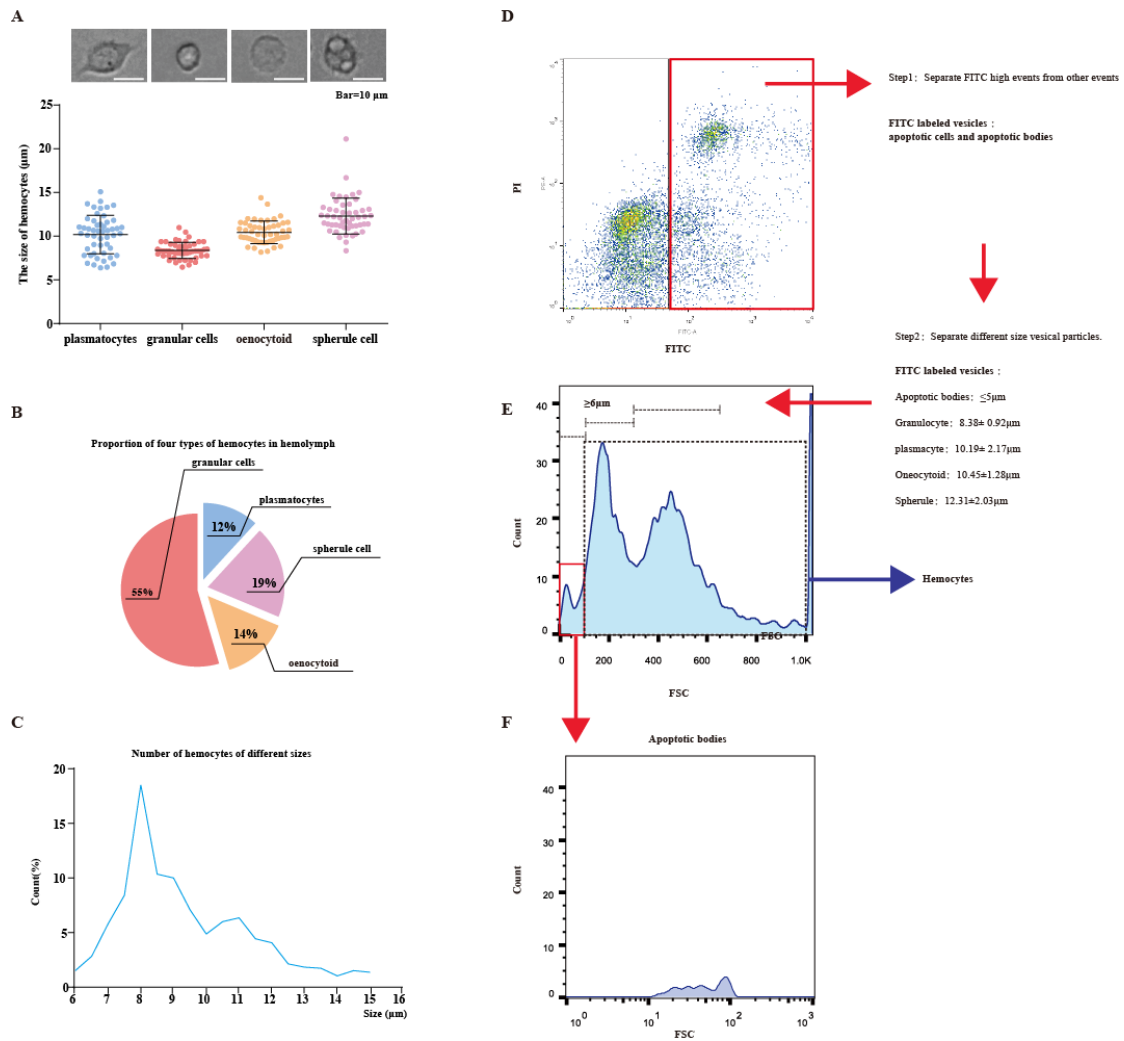67
68
69

**Protein levels in haemocytes after dsRNA feeding**

70
71

**Figure S2. dsRNA inhibited Inx proteins (Related to Figure 3).**

Western blotting of four Inx proteins from haemocytes isolated from host treated with

ds RNAi. ds*egfp* was used as a dsRNA control and GAPDH as a reference.

106

**Figure S3. Flow cytometry analysis of the number of apoptotic bodies (Related to Figure 3).**

(A) Size distribution of haemocytes of *Spodoptera litura*: Granulocyte, $8.38 \pm 0.92$ μm (n = 50); plasmacyte, $10.19 \pm 2.17$ μm (n = 50); Oneocytoid: $10.45 \pm 1.28$ μm (n = 50); Spherule, $12.31 \pm 2.03$ μm (n = 50). (B) Proportion of different blood cells in the haemolymph of *S. litura*. (C) Percentage of haemocytes of different sizes in *S. litura*. Different types of haemocytes were analysed according to their size to obtain a cell size ratio map with two peaks. (D) Screening of apoptotic cell populations of haemocytes of *S. litura* using flow cytometry. (E) Apoptotic cell population containing apoptotic bodies and apoptotic cells, identified by peak and FSC, compared with the line graph of the percentage of cell size calculated by microscopy. The apoptotic body population is indicated by the smallest peak. (F) Number of apoptotic bodies.

4

**Figure S4. Innexins (Inxs) are substrates of caspase-3 activated by MbBV (Related to Figure 3).**

(A and B) Western blot of Inx2/3 cleaved by active caspase-3. (C and D) Western blot of Inx2/3 cleaved by active caspase-3 and MbBV. (E and F) Western blot of Inx2/3 cleaved by MbBV. **$p < 0.01$. Unpaired Student's $t$-test using the Holm-Sidak method for multiple $t$-test; n = 3. IgG was used as a reference.

**Table S1. The location of Inx genes in bracovirus integrated *Spodoptera litura***

**genome (Related to Figure 2).**

| ID | Name | CDS length (bp) | Position | MbBV DNA integration nearby |
|---|---|---|---|---|
| SWUS10010590 | *inx1* | 1086 | Chr 2 | HIM-C16, HIM-F157 |
| SWUS10010610 | *inx2* | 1080 | Chr 2 | HIM-C16, HIM-F157 |
| SWUS10043510 | *inx3* | 1161 | Chr 9 | HIM-C16, HIM-C14, HIM-F157 |
| SWUS10127310 | *inx4* | 1116 | Chr 29 | HIM-C16, HIM-F157 |

137

138
139
140
141
142
143
144
145
146
147
148
149
150
151
152
153
154
155
156
157
158
159
160
161

162 **Table S2. Inx proteins in *Spodoptera litura* haemocytes parasitised by *Microplitis***
163 ***bicoloratus* (Related to Figure 2).**
164

| Accession | Name | M/S results | Protein Mass | Protein Length | % Cov (95) | Unique Peptides | Unique Peptide Sequence |
|---|---|---|---|---|---|---|---|
| comp88846_c0_seq1 | Inx1 | / | / | / | / | / | / |
| comp65035_c0_seq1 | Inx2 | / | 41526.3 | 360 | 8.635000139 | 2 | MLVLDLNCPVVGDECKDSR; LAPQAQVEAVAR |
| Comp99381_c0_seq1 | Inx3 | down | 43965.8 | 387 | 15.02999961 | 5 | GIAHPGLGNDFEEEKR; LVQYLVDTR; TDPMIEVFPR; VFGEVLDELSR; FGTPAGVESLVR |
| Comp121018_c0_seq1 | Inx4 | / | / | / | / | | / |

165
166
167
168
169
170
171
172
173
174
175
176
177
178
179
180
181
182
183
184
185
186
187
188
189

**Transparent Methods**

**Reagents.** TO-PRO-3 was purchased from Invitrogen (Thermo Fisher, T3605, Eugene, OR， America). Annexin V-FITC/PI was purchased from Solarbio (Solarbio, CA1020, Beijing, China). PI was purchased from Sigma. Activated caspase-3 was purchased from Cayman (Michigan, 10010209), and CBX was purchased from Sigma.

**Microscopy.** Time-lapse live imaging was performed at 27 °C using a Leica DMi8LASX microscope with a 20× objective lens.

**Insect rearing and virion isolation.** To identify the apoptotic bodies of haemocytes parasitised by *Microplitis bicoloratus*, *Spodoptera litura* was reared as described previously (Luo and Pang, 2006; Luo et al., 2007).

**Cell culture.** Sf9 (IPLB-Sf21-AE) cells were derived from *S. frugiperda* pupal ovarian tissue (Vaughn et al., 1977), and adherent Spli221 (TUAT-Spli221) cells were derived from *S. litura* (Yanase et al., 1998) cultured in TNM-FH insect culture medium supplemented with 10% foetal bovine serum (Hyclone, Logan, UT, USA).

**Apoptotic bodies.** To identify the apoptotic bodies of haemocytes, 100 μL of a suspension of haemocytes isolated from *S. litura* larvae was mixed with 500 μL of chilled 1× PBS and dispensed in 12-well plates, followed by incubation for 20 min. Once all haemocytes adhered to the bottom of the plate, the cells were labelled using

213  an Annexin/PI kit purchased form Solarbio (CA1020, Beijing, China). Five images per

214  recorded per 12-well plate using the 20× objective lens (both bright and fluorescent

215  fields) of an inverted fluorescence microscope (Olympus 1X71) at room temperature.

216  Vesicles < 5 μm in size were defined as apoptotic bodies. The total number of cells in a

217  single image was counted; five images were acquired per experiment.

218      Time-lapse microscopy was used to analyse apoptotic body formation during

219  different treatments with MbBV and reBac-TEV-Inxs. After 2 h of incubation of $1 \times$

220  $10^6$ cells/well in 6-well plates (Nest, 703001), MbBV was added to the plates, and five

221  images were recorded per plate using the 20× objective lens (both bright and fluorescent

222  fields) at 30-min intervals for 72 h using a live-cell imaging system (Leica,

223  DMi8LASX). LAS X software was used to analyse and record the number of cells

224  forming apoptotic bodies. The percentage of apoptotic bodies = (apoptotic bodies/total

225  cell number)/100.

226

227  **Flow cytometry gating for apoptotic bodies**. The *S. litura* haemocytes were stained

228  with Annexin V-FITC/PI. Flow cytometry analysis helped sort a subpopulation of cells

229  with high FITC staining, which included apoptotic cells and apoptotic bodies. Next, the

230  high FITC cell subpopulation was analysed using FSC and Count as the horizontal and

231  vertical coordinates, to detect three peaks within the cell population. Comparison of the

232  haemocyte data using microscopy confirmed that the FSC value was within the

233  expected range of 100-1.0 k, similar to the distribution of a normal haemocyte

234  population. The FSC values under the first and second count peak should be

235    approximately equal to 8 and 11 µm, respectively, whereas the FSC value corresponding

236    to the first count value is approximately equal to 6 µm. In addition, each particle group

237    with a complete membrane structure with a size ≤ 5 µm was identified as an apoptotic

238    body group.

239

240    **Induction of apoptosis.** For *in vivo* experiments, the haemocytes of *S. litura* were

241    parasitised by *M. bicoloratus*. For *in vitro* experiments, Sf9 cells in TNM-FH

242    supplemented with 10% FBS were treated with 1–9 wasp equivalents of bracovirus or

243    1%–5% reBac-TEV-Inxs for 12–72 h.

244

245    **Dye uptake via hemichannels.** To measure dye uptake by apoptotic cells treated with

246    viruses, the cells were incubated with TO-PRO-3 (Thermo Fisher, T3605，Eugene, OR，

247    America) for 15 min at room temperature. Five images were recorded per plate using

248    the 20× objective lens (both bright and fluorescent fields) of an inverted fluorescence

249    microscope (Olympus 1X71) at room temperature. PI uptake by apoptotic cells treated

250    with MbBV was measured at 4 °C, as described previously (Luo and Turnbull, 2011).

251    Briefly, $1 \times 10^4$ cells, treated as indicated, were seeded in 96-well plates and incubated

252    at 4 °C for 2 h. This was followed by incubation with 50 µg/mL of PI for 5 min at 4 °C.

253    The cells were fixed for 15 min with 3.7% formaldehyde, and five images were

254    recorded per plate using the 20× objective lens (both bright and fluorescent fields) of

255    an inverted fluorescence microscope (Olympus 1X71, Tokyo, Japan) at room

256    temperature.

257

**Genome analysis of MbBV-infected cells.** To scan for fragments of MbBV integrated

into the host genome, we sequenced DNA isolated from 6-day parasitised haemocytes

and MbBV-infected Spli221 cells. Host integration motifs (HIMs) from Microplitis

demolitor bracovirus (Burke et al., 2014) were used to scan chromosomes 2, 9, and 29,

where Inx1, Inx2, Inx3, and Inx4 are localised. The MbBV genome sequence was

compared with these sequences.

264

**Proteomics of parasitised haemocytes.** To examine the expression of *inx* genes after

parasitisation, the parasitised haemocytes were isolated, and protein sequences for Inx

1–4 were determined using tandem mass spectrometry.

268

**qRT-PCR.** Total RNA was isolated from five samples using RNAiso Plus (TaKaRa,

Dalian, China), according to the manufacturer's instructions, followed by DNase

treatment. The concentration and purity of each RNA sample were determined by

measuring the optical density ratio A260/A280 using a NanoDrop 2000. Samples with

an A260/A280 ratio > 2.0 were used to synthesise cDNA using a 5× All-In-One RT

MasterMix Kit (abm, Vancouver, Canada) according to the manufacturer's instructions.

All cDNA samples were stored at −80 °C for preservation. qRT-PCR was performed

using cDNA and the following primers: Q-Inx1-F (5'- GCG GTA GAG CGG ACA C -

3'), and Q-Inx1-R (5'- CGT GAT GCG AGG GAA TA -3'); Q-Inx2-F (5'-CGT TCC

GTT TCT TTA TCT G-3'), and Q-Inx2-R (5'- ACA CGC TCC TCT GGC TC-3'); Q-

279    Inx3-F (5'-ATC GCA TCA CAT CAG CC-3'), and Q-Inx3-R (5'-AGG TAA TCC AGC

280    AAT AGG-3'); Q-Inx4-F (5'- AAG ACG CCA TCA ACA GC -3'); Q-Inx1-R (5'- GCC

281    GAG CAG CAC AAA -3'); Q-18S-F (5'-AGA ACT CTG ACC AGT GAT GGG ATG-

282    3'), Q-18S-R (5'-CTG ATT CCC CGT TAC CCG TGA-3'). We used EvaGreen 2×

283    qPCR MasterMix (Abm, MasterMix, Richmond, Canada) with the following

284    recommended cycling parameters: 95 °C, 30 s; 95 °C, 5 s, 60 °C, 34 s, 40 cycles; 95 °C,

285    15 s; 60 °C, 1 min; 95 °C, 15 s. The 18S rDNA gene was used as the reference gene. To

286    quantify the relative mRNA levels of each target gene, each sample was tested in

287    triplicate, and the $2^{-\Delta\Delta CT}$ method was used as previously described (Livak and

288    Schmittgen, 2001).

289

290    **Gene knockdown.** siRNAs were used to knock down the genes of interest. The siRNAs

291    were synthesised by GenePharma (GenePharma, Suzhou, China). The sequences were

292    as follows: siRNA-*inx*1-F (5'-GGA CUG AUA AUG CAG UGU UTT-3'), and siRNA-

293    *inx*1-R (5'-AAC ACU GCA UUA UCA GUC CTT-3'); siRNA-*inx*2-F (5'-GGU GAA

294    AUA CCA CAA GUA UTT-3'), and siRNA-*inx*2-R (5'-AUA CUU GUG GUA UUU

295    CAC CTT-3'); siRNA-*inx*3-F (5'-GGA GGU GCU UUC UUG ACA UTT-3'), and

296    siRNA-*inx*3-R (5'-AUG UCA AGA AAG CAC CUC CTT-3'); siRNA-*inx*4-F (5'-

297    GCG AGA AGG ACA GUG AUA ATT-3'), and siRNA-*inx*4-R (5'-UUA UCA CUG

298    UCC UUC UCG CTT-3'). CRISPR/Cas9 was used to knock out the gene of interest;

299    gRNAs were designed using the resource available at http://sidirect2.rnai.jp. To knock

300    down gene expression *in vivo*, dsRNA plasmids were constructed as described

301 previously (Timmons et al., 2001). Briefly, the gene sequences were clone into an

302 L4440RNAi vector containing two convergent T7 polymerase promoters that were

303 oppositely oriented and separated by a multicloning site. The plasmids were sequenced,

304 and the correctly cloned plasmids were used to transform *Escherichia coli* HT115

305 (DE3), which was the bacterial host. Bacteria transformed with EGFP RNAi served as

306 negative controls.

307

308 **Western blotting.** Western blotting was performed as previously described (Liu et al.,

309 2013). Briefly, the cultured cells were lysed using RIPA lysis buffer (cat. no. R0100;

310 Solarbio, Beijing, China), and the protein concentrations were measured using a BCA

311 protein quantification assay kit (cat. no. BCA02; Dingguo, Beijing, China). Samples

312 (50 µg) were separated by SDS-polyacrylamide gel electrophoresis and transferred to

313 PVDF membranes. After incubation with antibodies, the bands were visualised using

314 enhanced chemiluminescence (Beyotime).

315

316 **Caspase-3-mediated cleavage of Inxs.** Inx proteins were isolated by incubating anti-

317 Inx2 and anti-Inx3 antibodies with cell lysates, followed by incubation with protein

318 A+G agarose beads (Beyotime, cat no. P2012) according to the manufacturer's protocol.

319 The isolated Inx proteins were incubated with active caspase-3 peptide (C10010209,

320 Cayman) at 37 °C and subjected to western blotting after 12–16 h.

321

322 **TEV-Inxs and TEV protease.** reBac-TEV-Inxs and reBac-Flag-TEV protease (N-

323 terminally elongated bacmids) were constructed based on previously described reports

324 (Chen et al., 2016; Guo et al., 2015). Briefly, pFastBacTM HTA vector (Invitrogen,

325 Carlsbad, CA, USA), which contained a Tobacco Etch Virus (TEV) cleavage site, was

326 used to construct reBac-TEV-Inxs. pFastBac1 containing a Flag tag was used to

327 generate pFasBac1-TEV protease. The plasmids were used to transform competent *E.*

328 *coli* DH10Bac cells (Gibco), and positive colonies were selected according to the

329 manufacturer's protocol. The same methods were used to generate reBac-TEV-Inx1 and

330 Inx4.

331

332 **Determining the volumes of high-titer bac-to-bac virus by cell cycle arrest**

333 Recombinant viruses were generated, and the volume of each high-titre virus was

334 determined using cell cycle arrest (Boukarabila et al., 2009). In brief, for the production

335 of the P1 viral supernatant, Sf9 cells in the mid-log phase growth were transfected with

336 the bacmid. At 72 h after transfection, the supernatant (P1 virus) was isolated. For the

337 production of the P2 viral supernatant, 10 mL of the Sf9 cell culture ($1.0 \times 10^6$ cells/mL)

338 was added to a cell culture flask; 30 min after cell adhesion, 5% (500 μL) P1 virus was

339 added into the flask (If the cells stopped doubling at 24 h, we deduced that excess P1

340 virus had been added. The process was then repeated using 1% virus. In contrast, if the

341 cells did not stop dividing by 48 h, the procedure was repeated using 10% P1 viral

342 supernatant). At 72 h after the P1 virus infection, the cells were centrifuged at $500 \times g$

343 for 5 min and the supernatant (P2 virus) was recovered. For preparing the P3 viral

344 supernatant, a large volume of mid-log phase cells (10 mL, $1.0 \times 10^6$ cells/mL) were

345 infected with 0.1% (10 μL) P2 virus supernatant. The cells were counted every 24 h for

346 72 h (if the cells stopped doubling at 24 h, we deduced that excess P1 virus had been

347 added, and the process was then repeated using 0.05% virus. In contrast, if the cells did

348 not stop dividing by 48 h, the process was repeated using 0.5% P2 virus). After 72 h,

349 the cell suspension was centrifuged at $500 \times g$ for 5 min to recover the supernatant (P3

350 virus). To induce cell apoptosis, 1% of the P3 virus supernatant was used, and 5% of

351 the P3 virus supernatant (MOI of 5% P3 virus $\approx$ 1) was used to induce the formation

352 of apoptotic bodies.

353

**Statistical analyses.** Data were analysed using GraphPad Prism (ver. 7, Prism), and

statistical significance was determined using the Student's *t*-test for unpaired

experiments (two-tailed). $p < 0.05$ was considered to indicate statistically significant

difference between groups. The resulting data are presented as means ± SEM from at

least three independent experiments.

**Supplemental References**

Boukarabila, H., Saurin, A.J., Batsche, E., Mossadegh, N., van Lohuizen, M., Otte, A.P., Pradel, J., Muchardt, C., Sieweke, M., and Duprez, E. (2009). The PRC1 Polycomb group complex interacts with PLZF/RARA to mediate leukemic transformation. Genes Dev. *23*, 1195-1206.

Burke, G.R., Walden, K.K.O., Whitfield, J.B., Robertson, H.M., and Strand, M.R. (2014). Widespread genome reorganization of an obligate virus mutualist. PLoS Genet. *10*, e1004660.

Chen, Y.-B., Xiao, W., Li, M., Zhang, Y., Yang, Y., Hu, J.-S., and Luo, K.-J. (2016). N-terminally elongated SpliInx2 and SpliInx3 reduce baculovirus-triggered apoptosis via hemichannel closure. Arch. Insect Biochem. Physiol. *92*, 24-37.

Guo, L.E., Zhang, J.F., Liu, X.Y., Zhang, L.M., Zhang, H.L., Chen, J.H., Xie, X.G., Zhou, Y., Luo, K.-J., and Yoon, J. (2015). Phosphate ion targeted colorimetric and fluorescent probe and its use to monitor endogeneous phosphate ion in a hemichannel-closed cell. Anal. Chem. *87*, 1196-1201.

Livak, K.J., and Schmittgen, T.D. (2001). Analysis of relative gene expression data using real-time quantitative PCR and the $2^{-\Delta\Delta CT}$ method. Methods *25*, 402-408.

Luo, K., and Turnbull, M.W. (2011). Characterization of nonjunctional hemichannels in caterpillar cells. J. Insect Sci. *11*, 6.

Luo, K.-J., and Pang, Y. (2006). Spodoptera litura multicapsid nucleopolyhedrovirus inhibits Microplitis bicoloratus polydnavirus-induced host granulocytes apoptosis. J. Insect Physiol. *52*, 795-806.

Luo, K.-J., Trumble, J.T., and Pang, Y. (2007). Development of *Microplitis bicoloratus* on *Spodoptera litura* and implications for biological control. BioControl *52*, 309-321.

Timmons, L., Court, D.L., and Fire, A. (2001). Ingestion of bacterially expressed dsRNAs can produce specific and potent genetic interference in *Caenorhabditis elegans*. Gene *263*, 103-112.

Vaughn, J.L., Goodwin, R.H., Tompkins, G.J., and McCawley, P. (1977). The establishment of two cell lines from the insect *Spodoptera frugiperda* (Lepidoptera; Noctuidae). In Vitro *13*, 213-217.

Yanase, T., Yasunaga, C., and Kawarabata, T. (1998). Replication of *Spodoptera exigua* nucleopolyhedrovirus in permissive and non-permissive lepidopteran cell lines. Acta Virol. *42*, 293-298.